Journal of Statistical Physics, Vol. 70, Nos. 1/2, 1993

Dynamics of Oscillators with Periodic Dichotomous Noise

Raymond Kapral[1] **and Simon J. Fraser**[1]

The dynamics of bistable oscillators driven by periodic dichotomous noise is described. The stochastic differential equation governing the flow implies smooth trajectories between noise switching events. The dynamics of the two-branched map induced by this flow is a Markov process. Harmonic and quartic models of the bistable potential are studied in the overdamped limit. In the linear (harmonic) case the dynamics can be reduced to a stochastic one-dimensional map with two branches. The moments decay exponentially in this case, although the invariant measure may be multifractal. For strong damping, relaxation induces a cascade leading to a Cantor set and anomalous decay of the density in this case is modeled by a Markov chain. For the physically more realistic case of a quartic potential many additional features arise since the contraction factor is distance dependent. By tuning the barrier-height parameter in the quartic potential, noise-induced transition rates with the characteristics of intermittency are found.

KEY WORDS: Stochastic differential equations; Markov chains; stochastic nonlinear maps; forced oscillators.

1. INTRODUCTION

It is a well-known fact that nonlinear oscillators which are subjected to periodic or random driving forces can display complex dynamics with unusual features. Both periodically forced nonlinear oscillators and oscillators with random white or colored noise sources have been studied in a variety of contexts (see, e.g., ref. 1). Stochastic resonance[2] is an example where both periodic and stochastic elements combine to give rise to new dynamical features.

[1] Chemical Physics Theory Group, Department of Chemistry, University of Toronto, Toronto, Ontario, Canada M5S 1A1.

0022-4715/93/0100-0061$07.00/0

A rather simple class of randomly perturbed oscillators is studied in this paper. We consider dynamical systems described by the equation of motion

$$m\ddot{x}(t) = -\zeta\dot{x}(t) - \frac{dV(x(t); v(t))}{dx(t)} \tag{1}$$

or, in the overdamped limit,

$$\dot{x}(t) = -\zeta^{-1}\frac{dV(x(t); v(t))}{dx(t)} = F(x(t); v(t)) \tag{2}$$

Here m is the mass of the "particle" and ζ is the friction coefficient.

The potential $V(x; v(t))$ is governed by a periodic dichotomous noise process on a parameter $v(t)$ that determines the form of the potential function. More specifically, $v(t)$ is given by

$$v(t) = \sum_{n=0}^{\infty} v(n)\,\theta(t - n\tau)\,\theta((n+1)\tau - t), \qquad t \geqslant 0 \tag{3}$$

where $\{v(n),\ n = 0, ..., \infty\}$ are independent random variables with probabilities such that $P(v(n) = v_0) = p$ and $P(v(n) = v_1) = 1 - p = q$, $\forall n$, and $\theta(x)$ is the Heaviside function. Note that in this noise process we set the zero of time at the instant of switching. The noise is correlated over the time interval τ and has correlation function

$$\langle v(t)\, v(0)\rangle = \begin{cases} (pv_0^2 + qv_1^2) & \text{for } t \leqslant \tau \\ (pv_0 + qv_1)^2 & \text{for } t > \tau \end{cases} \tag{4}$$

This noise process is easily implemented by choosing the parameters v_0 and v_1 with probabilities p and q, respectively, at fixed time intervals τ. Thus, like stochastic resonance, the noise process combines random and periodic elements and gives rise to interesting dynamical behavior which is amenable to experimental test.[3,4]

The periodic element in the dynamics allows an analysis in terms of discrete-time maps. The equations of motion, Eq. (1) or (2), may be integrated over the time interval τ to yield a stochastic map. We restrict our study to overdamped dynamics. Integration of Eq. (2) yields

$$x(t+\tau) = x(t) + \int_t^{t+\tau} dt'\, F(x(t'), v(t')) \tag{5}$$

$$x(t+\tau) = \begin{cases} f^{\tau}(x(t), v_0) \equiv f_0^{\tau}(x(t)), & \text{prob. } p \\ f^{\tau}(x(t), v_1) \equiv f_1^{\tau}(x(t)), & \text{prob. } q \end{cases} \tag{6}$$

This stochastic map captures the essential features of the stochastic differential equation (2). Random walks on a lattice with disorder have also been described by random maps of the type considered here.[5]

For random switching between two harmonic potentials, our dynamical system, with strong damping, reduces to a stochastic linear one-dimensional map[3,4] Its two branches f_0^τ and f_1^τ are defined by

$$\begin{aligned} f_0^\tau &: \quad x(t+\tau) = \lambda x(t), && \text{prob. } p \\ f_1^\tau &: \quad x(t+\tau) = 1-\lambda+\lambda x(t), && \text{prob. } q \end{aligned} \tag{7}$$

where $\lambda = \exp(-m\omega^2\tau/\zeta)$ with ω the oscillator frequency. We sketch the mathematical history of this system because it shows how an infinitely recursive mathematical structure[6] can appear as an interesting new model in physics.

The dynamical process (7) on the unit interval was studied by mathematicians under the name "Bernoulli convolution."[7] Erdős and Salem showed that the invariant measure m^* of this process could have surprising properties, and even now the behavior of m^* for $\lambda \in [1/2, 1]$ is not fully understood.[8] For example, for $p = 1/2$, if λ is a reciprocal Pisot–Vijayaraghavan (PV) number[9] m^* is purely singular[7,10] i.e., the Lebesgue measure of the set on which the "mass" of the system is eventually concentrated is zero, but this set is dense, so that the graph of m^* increases continuously on this dense measure-zero set. (A PV number is an algebraic integer all of whose conjugates lie inside the unit circle in the complex plane.) Commonly a histogram of the corresponding coarse-grained "invariant" density is displayed to reveal the self-similarity of this structure, although, rigorously speaking, an invariant density does not exist in such cases.

The properties of m^* are far easier to grasp in the Cantor-set regime,[3] $\lambda \in (0, 1/2)$, and at $\lambda = 1/2$, where m^* is either absolutely continuous for $p = 1/2$ or a binomial multifractal[11] for $p \neq 1/2$.

For $\lambda \in (0, 1/2)$ and $p \in (0, 1)$ the support of m^* is the nowhere-dense Cantor set $\mathscr{C}_\lambda$ with similarity ratio λ and m^* is purely singular. The graph of $m^*(x; \lambda, p)$ is constant on the intervals corresponding to the gaps in the construction of $\mathscr{C}_\lambda$, Since $\mathscr{C}_\lambda$ has zero Lebesgue measure, the graph of m^* has zero derivative (and therefore vanishing density) almost everywhere in $[0, 1]$. Indeed, the decimation construction has a dynamical analog, as we shall see. This simple Cantor set structure should be contrasted with the graph of m^* for $\lambda \in (1/2, 1)$, which contains no intervals on which it is constant, even when m^* is purely singular and therefore concentrated on a dense measure-zero set.

In this article we examine properties of the invariant measure and relaxation dynamics for the system (2) when the potential is either a quadratic or quartic polynomial. In Section 2 we focus on the relaxation dynamics of the system with a harmonic potential. The relaxation properties are shown to be anomalous when viewed as discrete-state Markov process. Section 3 is devoted to the case where the potential is a quartic polynomial. We show how the invariant measure changes as a result of the nonlinear character of the stochastic map and describe noise-induced transition rate processes that arise from the nonlinear nature of the restoring force. Section 4 contains a discussion of the results.

2. HARMONIC POTENTIAL

In the Introduction we outlined some of the unusual properties of m^* for the system with a harmonic potential. The properties of m^* in the Cantor-set regime make it interesting to study the relaxation toward its purely singular equilibrium. This type of relaxation cascade is similar to recent models of turbulence using random multiplicative processes[12] and imitates the way "pre-fractals" arise in Mandelbrot's explanation of the properties of multifractal measures.

The relaxation dynamics for the map (7) is formally described by the Perron–Frobenius (PF) equation

$$\rho(x, t+\tau) = \int_{-\infty}^{\infty} dy \, \{ p\delta(x - f_0^{\tau}(y)) + q\delta(x - f_1^{\tau}(y)) \} \, \rho(y, t) \tag{8}$$

This discrete-time functional evolution equation implies the compression of the density ρ by factor λ to the left (with prob. p) and to the right (with prob. q). As indicated by the earlier discussion, this equation may not converge to a well-defined invariant density ρ^*, but an invariant measure $m^*(x; \lambda, p)$ always exists, as shown by Karlin.[7] Therefore the measure $m(x, t)$ evolving from any smooth initial $\rho(x, 0)$ approaches $m^*(x; \lambda, p)$ as $t \to \infty$.

2.1. Decay of Moments

Consider the time evolution of the moments

$$\langle x^m \rangle(t) = \int_{-\infty}^{\infty} dx \, x^m \rho(x, t) \tag{9}$$

under Eq. (8) when $\rho(x, 0)$ has support $[0, 1]$. This immediately gives

$$\langle x^m\rangle(t+\tau) = p\lambda^m\langle x^m\rangle(t) + q\sum_{n=0}^{m}\binom{m}{n}\lambda^n(1-\lambda)^{m-n}\langle x^n\rangle(t) \quad (10)$$

so that higher moments are coupled to lower ones. From Eq. (10) it follows that the first moment decays to its asymptotic value q with decay constant λ:

$$\langle x\rangle(t+\tau) - q = \lambda\{\langle x\rangle(t) - q\} \quad (11)$$

Similarly, the mth-order cumulant decays to its asymptotic value with decay constant λ^m. Thus, the decay of moments in this system is exponential, regardless of any singular structure $m^*(x; \lambda, p)$ might have.[2]

2.2. Markov Chain Model

Although the moments in this system decay normally, the density ρ shows anomalous relaxation behavior. The anomalous decay is best illustrated by a discussion of the Cantor-set regime, where the argument is clear.

The decimation process that generates $\mathscr{C}_\lambda$ also imitates the way density is swept out of the gaps at every iterate of the integral equation (8). This dynamics corresponds to a semigroup whose abstract structure arises from the decimation construction. Thus we can model this relaxation cascade by a hierarchy of finite Markov chains up to some chosen decimation level l, say. Each Markov chain in this cascade captures features of the relaxation in the decimation hierarchy. However, if we choose a definite value of l, it is impossible to represent the gap relaxation corresponding to previous levels because the semigroup structure of the relaxation dynamics manifests itself as defectiveness in the eigensystem of the Markov chain representation. We now formally examine the recursion leading to a particular decimation level l.

States in the chain are of two types: gap states $\mathscr{G}$ and support states $\mathscr{S}$, i.e., sets in which the mass must eventually reside. There are three kinds of allowed transition: $\mathscr{G} \to \mathscr{G}$, $\mathscr{G} \to \mathscr{S}$, and $\mathscr{S} \to \mathscr{S}$. The recursive construction of $\mathscr{C}_\lambda$ allows the eigensystem of the Markov chain to be defined completely. Starting from $\mathscr{P}_0 = \{\mathscr{S}_1\}$ with $\mathscr{S}_1 = [0, 1]$, the partition $\mathscr{P}_{l+1}$ can be generated from $\mathscr{P}_l$ according to the recursion

$$\mathscr{P}_{l+1} = \{f_0^\tau(\mathscr{P}_l), \mathscr{G}_{2^l+1}, f_1^\tau(\mathscr{P}_l)\} \quad (12)$$

[2] We thank J. Piasecki and M. Moreau for communications concerning the cumulant generating function in this case.

where the set of $f_1^{\tau}(\mathscr{P}_l)$ are renumbered by adding 2^{l+1}. Using this procedure, the $(2^{l+1}-1)$ interlaced $\mathscr{S}$ and $\mathscr{G}$ intervals (states in the discrete Markov chain) of $\mathscr{P}_l$ are numbered consecutively, i.e.,

$$\mathscr{P}_l = \{\mathscr{S}_1, \mathscr{G}_2, \mathscr{S}_3, ..., \mathscr{G}_{2^{l+1}-2}, \mathscr{S}_{2^{l+1}-1}\} \tag{13}$$

The stochastic matrix P_l for the Markov chain will be written with row sum equal to one, so that the "physical" eigenvectors are (left) row vectors. Transitions to the left have probability p and those to right have probability q. Because of the decimation defining $\mathscr{C}_\lambda$, p and q occur either singly or in vertical triplets in the $(2^{l+1}-1)\times(2^{l+1}-1)$ stochastic matrix P_l $(l>0)$, and this can be constructed as follows. To fill in the p entries, start at row 1, column 1:

S1. Write a column of p's for 3 rows; from last entry, move 1 column to the right and 1 row down.

S2. Write one (column) p for one row; from last entry, move 1 column to the right and 1 row down.

Repeat S1, then S2, until every row of P_l has a single p entry. To fill in the q entries, start at row 1, column 2^l+1. Now use S1 and S2 (with q instead of p) until every row of P_l has a single q entry. All other entries of P_l are 0. The sparse structure of P_l means that all the rows of $(P_l)^{l-1}$ equal the equilibrium eigenvector π_l^* (below). This linear dependence implies $(P_l)^{l-1}$ has eigenvalues $\mu=1$ and $\mu=0$, with multiplicity $(2^{l+1}-2)$, but since l is finite, these are also the eigenvalues of P_l.

The underlying decimation defining $\mathscr{C}_\lambda$ also allows the equilibrium and relaxation eigenvectors of P_l to be defined recursively as follows:

1. Using $\pi_0^*=(1)$ belonging to $\mu=1$ for $P_0=1$ as initialization, the equilibrium eigenvector π_{l+1}^* is defined recursively in terms of π_l^* by $\pi_{l+1}^*=(p\pi_l^*, 0, q\pi_l^*)$, where each occurrence of π_l^* is a row vector of $2^{l+1}-1$ elements, making π_{l+1}^* a row vector of $2^{l+2}-1$ elements. Note that π_l^* has 2^l positive entries interlaced with 2^l-1 zeros.

2. All the relaxation eigenvectors for P_{l+1} belonging to $\mu=0$ can be obtained from π_l^* by the following substitution: Any positive element in π_l^* is replaced by the triplets $(1, 0, -1)$ or $(1, -2, 1)$ and every other occurrence of a positive element is replaced by the zero triplet $(0, 0, 0)$. Since there are 2^l positive entries in π_l^*, we obtain 2^{l+1} linearly independent eigenvectors all belonging to $\mu=0$.

A crucial point of this construction, which derives all possible null-space eigenvectors for P_{l+1} from the preceding equilibrium π_l^*, is that the eigen-

system for every $l>1$ is defective. For P_l, which has dimension $2^{l+1}-1$, we can write

$$\text{defect}_l=(2^{l+1}-1)-2^l-1=2^l-2 \tag{14}$$

where the subtracted terms on the right correspond to the dimensions of the subspaces spanned by the $\mu=0$ and $\mu=1$ eigenvectors. The number defect_l counts those gap states appearing early in the decimation hierarchy for $\mathscr{C}_\lambda$, whose (density) relaxation dynamics *cannot* be represented in the eigenbasis. It is only the final step of the density relaxation that can be represented in this eigenbasis. Since it can take as many as l steps to reach equilibrium for the defective matrix P_l, relaxation is slow because $\mu=0$ is the only relaxation eigenvalue.

However, there is a further paradoxical feature of this Markov chain picture: Suppose that an initial state is represented in the natural basis on the gap state hierarchy; we know that such an initial state cannot be represented in the eigenbasis of P_l. Nevertheless, the decay of the moments, using the centroids of the gaps as weights, from such gap states lying entirely outside the eigenspace can be faithfully represented until the first $\mathscr{G}\to\mathscr{S}$ transition is made, i.e., until the eigenspace is reached.

This anomalous relaxation for the Markov-chain model in the Cantor-set regime suggests similar anomalies in the eigenspace of the PF operator even on arbitrarily small length scales. Only if the system is "noisy," so that there is a finite inner length scale, can the usual kind of relaxation or equilibrium eigenvectors be constructed, and even then the eigensystem is defective.

3. QUARTIC POTENTIAL

A more realistic and commonly used potential model for the study of noise-induced rate processes is the quartic potential

$$V(x)=\frac{1}{4}x^4-\frac{\varepsilon}{2}x^2-vx \tag{15}$$

In this section we study the overdamped motion of a particle in this potential subject to periodic dichotomous noise on the parameter v. The physical situation we wish to study is depicted in Fig. 1, which shows two potential functions corresponding to $v_0=-v$ and $v_1=v$. The value of v is chosen to be sufficiently large that each potential function possesses a single extremum and the periodic dichotomous noise process induces transitions between the two potential branches.

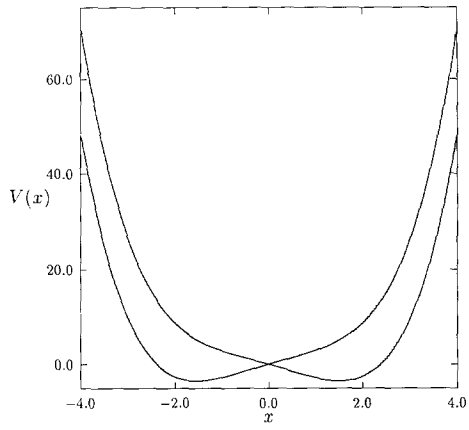

Fig. 1. Sketch of the potential function $V(x; \varepsilon, v)$ for $\varepsilon = 0.5$ and $v_{0,1} = \pm 2.8$.

The general overdamped equation of motion is given in Eq. (2) and for the quartic potential takes the specific (scaled) form

$$\frac{dx(t)}{dt} = -x(t)^3 + \varepsilon x(t) + v(t) \tag{16}$$

Integration of this equation over the time interval τ yields the stochastic map

$$x(t+\tau) = \begin{cases} C^\tau(x(t), v_0), & \text{prob. } p \\ C^\tau(x(t), v_1), & \text{prob. } q \end{cases} \tag{17}$$

As in Sections 1 and 2, we use the notation $C^\tau(x, v_i) = C_i^\tau(x)$ $(i = 0, 1)$. The integration in passing from Eq. (16) to Eq. (17) can be carried out to obtain a transcendental equation for $x(t+\tau)$ given $x(t)$:

$$\tau = -\frac{1}{A^{(i)}} \sum_{j=1}^{3} a_j^{(i)} \ln \frac{x(t+\tau) - x_j^{(i)}}{x(t) - x_j^{(i)}} \tag{18}$$

Here $x_j^{(i)}$ $(j = 1, 2, 3)$ are the roots of the cubic polynomials, $-x^3 + \varepsilon x + v_i = 0$ $(i = 0, 1)$, and

$$A^{(i)} = \sum_{j=1}^{3} x_j^{(i)} x_{j+1}^{(i)} (x_j^{(i)} - x_{j+1}^{(i)}) \tag{19}$$

and

$$a_j^{(i)} = x_{j+1}^{(i)} - x_{j+2}^{(i)} \tag{20}$$

where the subscript addition is carried out modulo 3. In the remainder of this section we shall focus attention on the symmetric case depicted in Fig. 1, where $v_1 = v = -v_0$, so that $x_j^{(0)} = -x_j^{(1)} = -x_j$, $A^{(0)} = -A^{(1)} = -A$, and $a_j^{(0)} = -a_j$ for $j = 1, 2, 3$. In this case the two maps $C_i^\tau(x)$ take a simpler form and are defined implicitly by

$$C_0^\tau: \quad \tau = -A^{-1} \sum_{j=1}^{3} a_j \ln \frac{x(\tau) + x_j}{x(0) + x_j}$$
$$C_1^\tau: \quad \tau = -A^{-1} \sum_{j=1}^{3} a_j \ln \frac{x(\tau) - x_j}{x(0) - x_j} \tag{21}$$

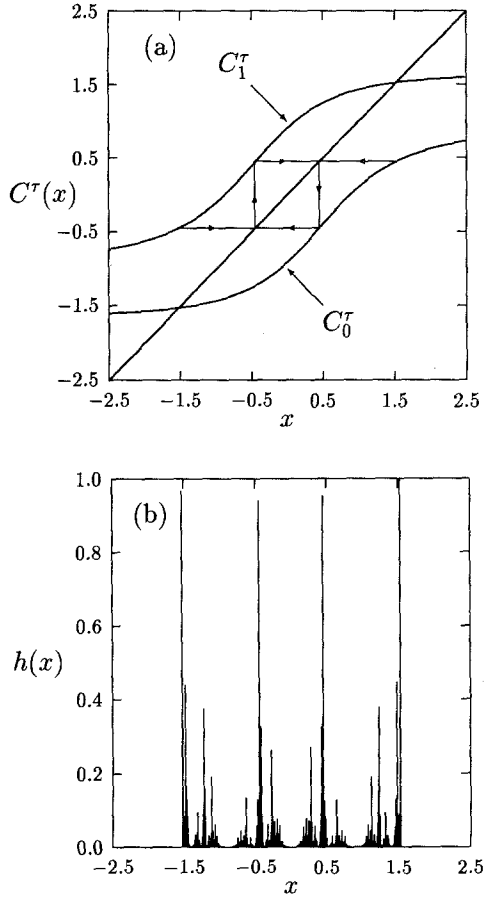

Fig. 2. (a) The two map branches $C_{0,1}^\tau(x)$ versus x for the parameter set of Fig. 1, $\tau = \tau_2 = 0.31967268$. Also shown is the period-two EPO. (b) Histogram $h(x)$ constructed from a trajectory of 6.26×10^5 points in 2000 bins.

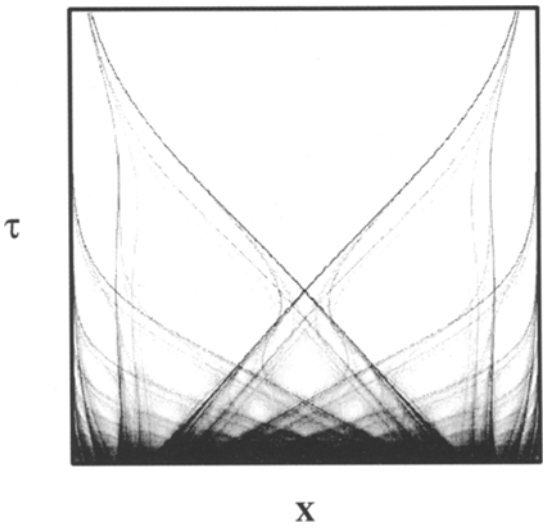

Fig. 3. Coarse-grained invariant density for the quartic potential. The abscissa is the interval $[-x_1, x_1]$, where $x_1 = 1.52745400$, and the ordinate is the interval [0.1, 1.1]. The normalized density decreases from black (one) to white (zero).

These are the basic mapping equations used in this study.[3] The discrete-time maps C_0^τ and C_1^τ are shown in Fig. 2a for $\varepsilon = 0.5$, $v = 2.8$, the same potential parameters as Fig. 1, and $\tau = 0.3196727$. To fix the notation, we denote the rightmost real fixed point of C_1^τ as x_1 while by symmetry the leftmost real fixed point of C_0^τ is $-x_1$.

An overview of the dynamical structure can be obtained from an examination of the coarse-grained density in Fig. 3. To construct this figure, the interval $[-x_1, x_1]$ was divided into 500 segments of equal length. The coarse-grained density on these segments was determined from the values of $x(n\tau)$ $(n = 1,..., T/\tau)$ along a stochastic trajectory of length $T = 20{,}000$. Results for 500 τ values in the range [0.1, 1.1] are shown.

The coarse-grained density is highly structured and some of its features are similar to those observed in the linear map case. The gross structure of this density is controlled by a few simple dynamical processes. Because of the flat regions of the map branches $C_{0,1}^\tau$ there is a strong focusing of the map iterates near the fixed points $\mp x_1$, respectively. As a result, the prominent features of the density can be attributed to the

[3] In carrying out some of the calculations we have found it convenient to integrate numerically Eq. (16) over the time interval τ instead of solving the nonlinear equation (21). However, Eq. (21) is useful in the theoretical analysis and in the determination of periodic orbits.

mapping of the endpoints $\pm x_1$ into the interior under simple sequences of iterates. Consider a sequence $\{i_1, i_2, ..., i_n\}$, $i_k \in \{0, 1\}$, where $i=0$ refers to iteration under C_0^τ while $i=1$ corresponds to C_1^τ. Sequences beginning with 0 have initial value $x(0)=x_1$, while those that begin with 1 have $x(0)=-x_1$. Figure 4 shows plots of $x(n\tau)$ as a function of τ for the sequences $\{i_1, i_2, ..., i_n\}$, $i_k=0$, $\forall k$, $n=1, ..., 5$, and $\{i_1, i_2, ..., i_n\}$, $i_k=1$, $\forall k$, $n=1, ..., 5$. These are shown as two sets of solid lines in the figure. Also shown as dotted lines are the sequences $\{011\}$, $\{010\}$, $\{001\}$ and $\{100\}$, $\{101\}$, $\{110\}$. The sets of solid and dotted lines form the skeleton of the prominent high-density regions in Fig. 3.

The crossing points of these skeletal lines correspond to high-density regions. The crossing points can be found by identifying the sequences of iterates discussed above. The first central crossing point is determined by the condition $\{0\}=\{1\}$ $[x(\tau)=0]$ or

$$\tau_c = -A^{-1} \sum_{j=1}^{3} a_j \ln \frac{x_j}{x_1 + x_j} \tag{22}$$

Above $\tau_c = 0.4846155$,

$$C_0^{\tau_c}([-x_1, x_1]) \cup C_1^{\tau_c}([-x_1, x_1]) \subset [-x_1, x_1]$$

and the "density" is defined on a Cantor set with many length scales due to the nonlinear character of the map. This region is the analog of the Cantor-set region of the linear map case.

Other prominent crossing points correspond to central periodic orbits (CPOs).[3,4] For example, the outermost crossing points of the solid skeletal lines in Fig. 4 are determined by the conditions $\{00\cdots0\}=\{1\}$

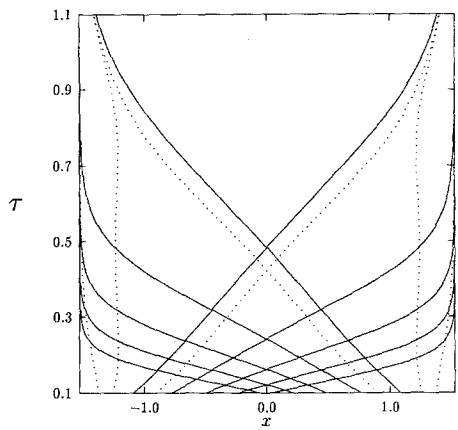

Fig. 4. Iterates of the fixed points as a function of τ form the skeleton of the coarsed-grained density.

and $\{11\cdots1\}=\{0\}$. These conditions correspond to the existence of period-$2n$ CPOs where the orbit is composed on n steps on the map branch C_0^τ and n steps on C_1^τ. The endpoints of the interval are mapped into the extreme points of the orbit forming a period-$2n$ eventually periodic orbit (EPO). The conditions for the existence of such orbits can be determined from

$$n\tau_n = -A^{-1}\sum_{j=1}^{3} a_j \ln\frac{x_j - x_n^*}{x_1 + x_j} \tag{23}$$

$$\tau_n = -A^{-1}\sum_{j=1}^{3} a_j \ln\frac{x_n^* + x_j}{x_1 + x_j} \tag{24}$$

Here x_n^* is one of the fixed points of the period-$2n$ orbit. The solutions of this equation are given in Table I up to $n=7$. The orbit endpoints tend to $\pm x_1$ and τ_n tends to zero as $n\to\infty$. As an illustration, the period-2 CPO is shown in Fig. 2a and the coarse-grained density in Fig. 2b. In contrast to the linear force case, the period-2 CPO is unstable and the map supports two stable period-2 orbits. However, it is the unstable CPO that controls the structure of the density due to the strong focusing of the map iterates near the endpoints of the interval. Notice the sharp maxima in the coarse-grained density at the fixed points of the period-2 orbit.

Another prominent family or orbits, referred to as the first family,[3,4] corresponds to crossings of the skeletal lines determined by the sequences $\{011\cdots10\}=\{1\}$ and $\{100\cdots01\}=\{0\}$. The period-4 orbit occurs at $\tau=0.454135340$ for $\varepsilon=0.5$ and $v=2.8$ with orbit elements $x_{1,2}^*=\pm0.084702127$ and $x_{3,4}^*=\pm1.2402225$. The orbit elements closest to the origin correspond to the two skeletal solid and dotted line intersections just below the central crossing point $\{0\}=\{1\}$ in Fig. 4.

Table I

n	x_n^*	τ_n
2	0.44698169	0.31967268
4	0.66656365	0.23836488
6	0.80090514	0.19090774
8	0.89369945	0.15982931
10	0.96261251	0.13785489
12	1.01629304	0.12146009
14	1.05954805	0.10873546

3.1. Noise-Induced Transitions

The parameters can be tuned so that the system is confined for long periods of time to the left and right of $x = 0$. In this circumstance "species" $s_{\mp}$ corresponding to the system in the left and right well can be identified and the characteristic relaxation times for the populations of these species can be computed.

One way to achieve slow leaking between the two halves of the phase space is to bring the two map branches near to tangency with the bisectrix. This case is illustrated in Fig. 5a for $p = 1/2$. Map iterates on the upper

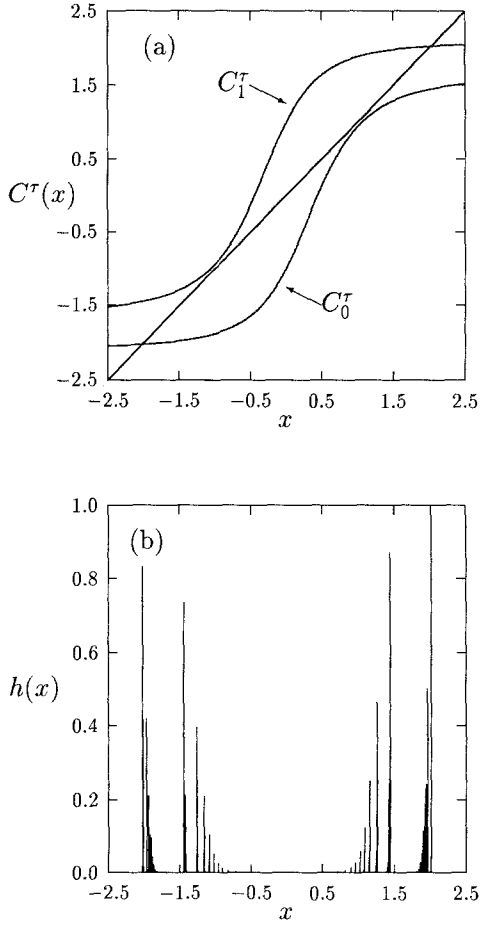

Fig. 5. (a) Map branches for a parameter set near tangent bifurcation: $\varepsilon = 3$, $\nu = 2.2$, and $\tau = 0.3$. (b) Histogram constructed from a trajectory of 6.26×10^5 points in 2000 bins.

(lower) branches will be closely spaced in the vicinity of the tangent point at negative (positive) x values. Stochastic transitions to the lower (upper) branch will result in phase points being mapped close to the fixed points at $-x_1$ (x_1), since the lower (upper) map branches are relatively flat near these fixed points. Transitions between s_+ and s_- can occur only through long sequences $\{00\cdots0\}$ or $\{11\cdots1\}$ since the system must pass through the narrow channel regions near the tangent points. Thus, a minimum number of steps on a given map branch is required for transition. When a noise-induced hop to the other map branch occurs the phase point will be reinjected into the vicinities of $\pm x_1$. This reflux process continues until passage through the channel occurs. The transition mechanism bears some similarity to intermittency.

The coarse-grained density constructed from the dynamics on the maps in Fig. 5a is shown in Fig. 5b. Sharp spikes in the density are seen at points corresponding to the deterministic steps through the channels near the tangent points of the upper (lower) map branches with the bisectrix. There are also images of these channel walks near the fixed points $\mp x_1$ produced by the mappings on the lower (upper) map branches. While the results presented in the figure show the effects of the finite relaxation time of the transitions between the left and right portions, it is clear that roughly one quarter of the density lies in each of the endpoint and tangent regions. Furthermore, the heights of the peaks decrease by a factor of two as iterates march through the channel, as expected, since there is a probability of one half of transition to the other map branch.

The probability density $P(t_{fp})$ of first passage times t_{fp} from $x(0) = -x_1$ to $x(t_{fp}) \geqslant 0$, with $x(t_{fp} - \tau) < 0$, is shown in Fig. 6. Apart from

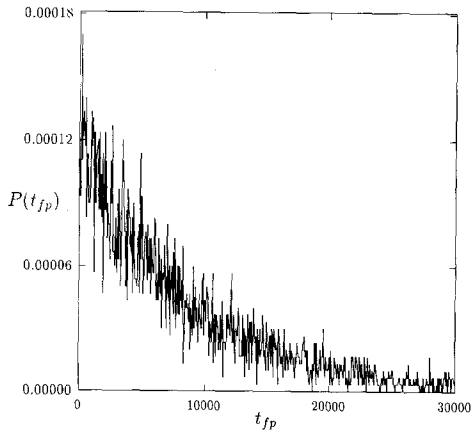

Fig. 6. Probability density function $P(t_{fp})$ for first passage time t_{fp} from the fixed point $x(0) = -x_1 = -2.0219013$ to $x(t_{fp}) \geqslant 0$, with $x(t_{fp} - \tau) < 0$, for the parameter set in Fig. 5.

fluctuations, the exponential form of P is evident, which is consistent with the uncorrelated character of the underlying stochastic process. However, starting from $-x_1$, a minimum of 12 steps is required to reach $x=0$. The mean first passage time $\langle t_{fp} \rangle = 24{,}619\tau$.

This brief examination of the transition process reveals a number of interesting features. The equilibrium state has a markedly discrete character, with mass dispersed in a roughly geometrical progression toward the species dividing point $x=0$. Decay from this type of distribution requires a new type of transition rate theory.

4. DISCUSSION

We have described a class of stochastic differential equations that, for a quartic potential in the overdamped limit, reduces to a two-branched nonlinear map in which each branch is a diffeomorphism. To gain insight into the dynamics, we have also analyzed a linear map corresponding to an underlying harmonic potential.

The linear model (with constant contraction factor λ) has been studied in the past for $p=1/2$; it is known to produce purely singular (multifractal) measures on a self-similar Cantor set when the images of $[0, 1]$ under the map branches do not overlap. A Cantor set structure is also produced in the nonlinear map if the branches do not "overlap" but now the Cantor set has nonconstant similarity ratio.

When the map branches overlap, a purely singular invariant measure m^* can arise in the linear case; this is known to occur when the λ is a reciprocal PV number. We have shown that such cases are also associated with eventually periodic orbits. Similarly, in the nonlinear case these EPOs organize the structure of m^*, but for a different reason; now the mass is concentrated near the points of the EPO because of the flatness and strong focusing effect of the map near the fixed points of its branches: Trajectories are repeatedly fed into the EPO from these fixed points, but no precise condition for purely singular measures is yet known for this nonlinear, overlapping case.

We have studied relaxation in the Cantor-set regime of the linear map using a discrete Markov-chain model. This demonstrates the way in which mass is swept irreversibly out of the gap hierarchy in the Cantor set; this annihilation cascade shows anomalies in the decay of the density. In contrast, the moments for density distributed on the gaps display exponential decay. This mixture of standard and anomalous features in the discrete case has important implications for the dynamics under the FP operator on the real line.

For the nonlinear map new features arise: In particular, trapping

induced by tangent bifurcation appears when the quartic potential acquires of local cubic inflection as two real roots collide. This trapping effect allows a "chemical reaction" description. In the parameter regime studied this "kinetics" is described as a first-passage-time problem.

This study demonstrates the variety of dynamical phenomena that can be produced by driving a simple deterministic system that responds slowly to a periodic dichotomous noise process. These phenomena are amenable to experimental verification in many physical systems.

REFERENCES

1. F. Moss and P. V. E. McClintock, eds. *Noise in Nonlinear Dynamical Systems* (Cambridge University Press, Cambridge, 1989), Vols. 1–3.
2. R. Benzi, S. Sutera, and A. Vulpiani, *J. Phys. A* **14**:L453 (1981).
3. A. J. Irwin, S. J. Fraser, and R. Kapral, *Phys. Rev. Lett.* **64**:2343 (1990).
4. S. J. Fraser and R. Kapral, *Phys. Rev. A* **45**(6) (March 1992).
5. C. Van Den Broeck and T. Tél, in *From Phase Transitions to Chaos: Topics in Modern Statistical Physics*, G. Györgyi, I. Kondor, L. Sasvári, and T. Tél, eds. (World Scientific, Singapore, to be published).
6. B. B. Mandelbrot, *The Fractal Geometry of Nature* (Freeman, New York, 1982).
7. P. Erdős, *Am. J. Math.* **61**:974 (1939); R. Salem, *Duke Math. J.* **11**:103 (1944); R. Salem, *Algebraic Numbers and Fourier Analysis* (Wadsworth, Belmont, 1983); S. Karlin, *Pac. J. Math.* **3**:725 (1953); A. M. Garsia, *Trans. Am. Math. Soc.* **102**:409 (1962); J.-P. Kahane, *Bull. Soc. Math. Fr.* **25**:119 (1971).
8. J. C. Alexander and J. A. Yorke, *Ergodic Theory Dynam. Syst.* **4**:1 (1984).
9. C. Pisot, *Annali Pisa* **7**:205 (1938); T. Vijayaraghavan, *Proc. Camb. Phil. Soc.* **37**:349 (1941); J. W. S. Cassels, *An Introduction to Diophantine Approximation* (Cambridge University Press, Cambridge, 1957), Chapter 8.
10. J. Stark, *Phys. Rev. Lett.* **65**:3357 (1990).
11. B. B. Mandelbrot, *Pure Appl. Geophys.* **131**:5 (1989).
12. A. B. Chhabra and K. R. Sreenivasan, in *New Perpectives in Turbulence* L. Sirovich, ed. (Springer-Verlag, Berlin, 1990); *Phys. Rev. A* **43**:1114 (1991).